Nonlinear lateral response of RC pile in sand: centrifuge and numerical modelling

Rui Zhao[1], *Anthony Kwan Leung[2], Jonathan Knappett[3], Scott Robinson[4], Andrew Brennan[5]

Abstract: Centrifuge modelling has been considered as an effective means of studying flexural soil-pile interaction, yet the conventional use of elastic material to model a reinforced concrete (RC) pile prototype is unable to reproduce the important nonlinear quasi-brittle behavior. It also remains a challenge to numerically model the soil-pile interaction due to the nonlinearity of both the soil and pile materials. This paper presents a small-scale model RC pile for testing soil-structure interaction under lateral pile-head loading in sand within a centrifuge. Accompanying non-linear finite-element numerical modelling is also presented to back-analyze the centrifuge observations and explore the influence of the constitutive models used. The physical model RC pile is able to (i) reproduce the pile failure mechanism by forming realistic tension crack patterns and plastic hinging and (ii) give hardening responses upon flexural loading. Comparisons of measured and predicted results demonstrate that for the laterally-loaded pile problem, the load-displacement response can be well approximated by models which do not incorporate strain softening, even though the soil behavior itself exhibits a strong softening response.

Keywords: Pile foundation; Reinforced concrete; Centrifuge modelling; Numerical modelling

Introduction

The design of piles against lateral loading is crucial for loads induced by wind, waves, and earthquakes (e.g., Bhattacharya et al. 2011; Anastasopoulos et al. 2013). It is a complex

[1] Postdoctoral Researcher, Center for Hypergravity Experimental and Interdisciplinary Research, Department of Civil Engineering, Zhejiang University, Hangzhou; Formerly Division of Civil Engineering, University of Dundee, Dundee
[2] Assistant Professor, Department of Civil and Environmental Engineering, Hong Kong University of Science and Technology, Hong Kong SAR. *Corresponding author; E-mail: ceanthony@ust.hk
[3] Professor, Division of Civil Engineering, University of Dundee, Dundee
[4] Postdoctoral Researcher, Division of Civil Engineering, University of Dundee, Dundee
[5] Senior Lecturer, Division of Civil Engineering, University of Dundee, Dundee

problem as it involves small-strain soil nonlinearity, and also large-strain (post-peak) strain softening in the case of dense (and hence dilative) sand. Geotechnical centrifuge modelling (e.g., Taylor 1995) has been employed as an effective means to study soil-pile interaction (e.g., Zhang et al. 1999). This technique enables small-scale physical models to be tested within an elevated gravity field, such that soil stress levels are the same as those experienced within much larger prototypes at homologous points. Based on this modelling technique and effective stress principle, it is possible to create an identical effective stress regime within a dry and a fully-saturated physical models by intentionally applying different g-levels to them.

A challenge of centrifuge testing of soil-pile interaction is to select an appropriate material that can correctly model the mechanical properties of the piles at prototype scale. Aluminum was a common modelling material (e.g., Zhang et al. 1999), for which either the stiffness or the strength could be scaled, but not both simultaneously. Moreover, it could not capture nonlinear pile behavior or cracking patterns that would be expected for reinforced concrete (RC) piles. RC has also been directly utilized to create pile models (e.g., Goode & McCartney 2015), but the coarse aggregate used without proper geometric scaling might lead to over-strength (Ito et al. 2006).

To overcome this limitation, Knappett et al. (2011) developed a small-scale model concrete, which was a mixture of plaster, water and fine sand. Fine sand was used to geometrically scale the coarse aggregates, so as to prevent the potential over-strength while realistically reproducing the nonlinear quasi-brittle behavior and having representative bending stiffness and moment capacity of RC pile prototypes. Recent modifications by Zhao et al. (2020) added copper powder to reproduce the thermal properties of concrete, for use in energy pile research. The small-scale model concrete has been successfully applied in the centrifuge to study the seismic behavior of pile-reinforced slopes, i.e. piles loaded by relative

45 soil–pile deformation (Al-Defae & Knappett 2014), but has not yet been used to physically
46 model laterally-loaded piles.

47 Due to the conventional use of elastic materials in physical modelling of piles, it was
48 commonly assumed that the pile behaves in a linear elastic manner when conducting
49 numerical back-analysis of model tests (e.g., Al-Baghdadi et al. 2017). Although this might be
50 a reasonable assumption for relatively small lateral pile displacements, when subjected to
51 large lateral displacements RC piles would exceed their elastic range and form plastic hinges
52 as tension cracks developed (Broms 1964). More sophisticated constitutive models are thus
53 necessary in order to capture such nonlinear response of model RC piles.

54 This paper studies the nonlinear behavior of a laterally-loaded RC pile in sand, combining
55 centrifuge modelling and three-dimensional numerical simulations. The numerical analysis is
56 conducted by employing the finite element (FE) method. Different soil constitutive models
57 are comparatively assessed, using the centrifuge model test results as a benchmark. The
58 degree of constitutive model sophistication is varied from simpler models to more
59 sophisticated ones, capturing stress- and/or strain-dependency of small-strain response, to
60 models incorporating post-peak strain softening. The importance of modelling the nonlinear
61 quasi-brittle response of RC piles, as well as the post-peak softening response of dilative soil
62 is highlighted and discussed.

63 **Centrifuge modelling**

64 Two centrifuge tests were conducted to study the behavior of laterally-loaded RC piles of
65 1/35th scale (i.e., scale factor, N = 35), installed in dry and saturated sand with the respective
66 density of ρ_{dry} and ρ_{sat} (denoted as Tests D and S). The g-levels adopted in Tests D and S
67 were 22-g and 35-g (denoted as g_{dry} and g_{sat}), respectively. Hence, the effective confining
68 stress acting on the 1:35 scaled piles in both tests was identical ($\rho_{dry} g_{dry} z = \rho_{sat} g_{sat} z$). This

technique of using the dry test at lower g to match the effective stress at higher g has previously been applied in centrifuge testing of piles by Li et al. (2010). Both centrifuge tests in the present study were performed using the 3.5-m-radius geotechnical beam centrifuge of the University of Dundee, U. K. (Brennan et al. 2014). A list of scaling laws relevant to this study is summarized in Table. 1. Note that for Test D, although the g-level applied was 22-g, when scaling up to prototype the scale factor of 1:35 was used because the model pile had effective stresses in the soil consistent with 1:35 scale. From this point onwards, all parameters were subsequently given at model scale, unless otherwise stated.

Model RC piles

Each model RC pile was produced using the model concrete created by Knappett et al. (2011), as later modified by Vitali et al. (2016) and Zhao et al. (2020). The model concrete used in the tests was made of β-form surgical plaster (Saint-Gobain Formula UK), fine sand (HST 95 Congleton silica sand) and water with a ratio of 1:1:0.9. Zhao et al. (2020) added 6% copper powder to the mix for tuning the thermal properties when the model concrete was used to model an energy RC pile. Although the present study does not focus on thermal effects (i.e., no temperature change was imposed in either of the centrifuge tests), the mix proposed by Zhao et al. (2020) was adopted for future comparison against energy RC pile behavior. The surface roughness of the model pile was measured to be 5.09 ± 0.93 μm, obtained by a surface roughness tester (0.01 μm resolution; SJ 201; Mitutoyo). This value was normalized by the d_{50} of the sand chosen for investigation in this study (0.13 mm), and the normalized roughness (R_n) is 0.0392.

The design bending moment capacity of the 10.5 m long RC pile of the prototype problem was 200 kNm. To meet this design criterion at the scale of 1:35, a square pile cross section of 18 x 18 mm^2 was required (Fig. 1a). Four 1 mm-diameter longitudinal reinforcing wires were

adopted, corresponding to a reinforcement ratio of 1.0% (by area). In addition, ten 0.63 mm-diameter transverse shear links were added to form a cage and used to fix flexible silicone pipes used for the thermal circuit. All steel reinforcement was modelled using a wire made of stainless steel (Ormiston Ltd., UK; Grade 316), which has a yield strength of 461 MPa and a Young's modulus of 190 GPa (Al-Defae & Knappett 2014). After pile production, four-point bending tests (FPB; BS EN 12390-5:2000) on three replicated piles showed that the range of prototype moment capacity (M_{ult}) and flexural stiffness (E_pI_p, where E_p is the Young's modulus of the pile and I_p is the second moment of inertia of the pile) were 219 – 231 kNm and 89 – 143 MNm^2, respectively. The prototype M_{ult} of the model pile (i.e. 225 ± 8 kNm; mean ± standard deviation) was close to the design value (i.e. 200 kNm) and also the yield strength determined by the normalized axial load (N)-bending moment (M) interaction diagrams of square columns from Eurcode 2 (taking N as zero). A typical Young's modulus (E) of real RC is approximately 30 GPa (Eurocode 2; EN1992-1-1). For a given pile width of 0.63 m, the second moment of inertia (I) is 0.004468 m^4, after discounting the presence of the internal pipes. Hence, the uncracked flexural stiffness of typical prototype piles is approximately 135 MNm^2, which is reasonably close to the prototype E_pI_p of the model pile (i.e. 116 ± 38 MNm^2).

Model preparation and soil properties

The model pile in each test was installed "wished-in-place" in a uniform bed of dense sand by suspending it and pluviating sand around it (in air). HST95 Congleton fine silica sand was used, of which the mechanical properties are summarized in Al-Defae et al. (2013). The ratio of pile width (D) to particle size (d_{50}) was more than 30, so particle size effects on pile behavior could be neglected (Bolton et al. 1999). An average sand relative density (D_r) of 67% was achieved in both tests. Key properties of the sand were summarized in Table 2. After sand

pluviation, the pile embedment depth was 250 mm (approximately $13D$), leaving the top 50 mm (approximately $3D$) above the soil surface (Fig. 2). The distance between the front face of the pile to the boundary of the soil container was more than $13D$, so no boundary effect on the pile lateral performance should be expected (Al-Baghdadi et al. 2017). To saturate the soil model for Test S, the bottom of the model package was connected to a water reservoir, and the water elevation was increased in steps. Model saturation was deemed to have been achieved when a water ponding of 10 mm was formed on the model surface.

Loading system, instrumentation, and test procedure

A bespoke lateral loading system was designed to apply displacement-controlled lateral (pushover) loading to the model pile. The system consists of a servo motor and a linear drive, which could provide a maximum loading rate of 3.1 mm/s over a stroke of 300 mm. To monitor the lateral deflection of the pile head, a draw wire potentiometer was used. A load cell was fixed on the axis of the drive shaft to measure the lateral load. In each test, the model package was spun up to $22g$ or $35g$ (as appropriate) in stages. Then, the motor was activated to conduct a displacement-controlled test at 0.7 mm/min (equivalent to 0.02 mm/min at prototype). For the coefficient of consolidation (c_v) of the sand (0.0615 m^2/s), the loading rate (v) of 0.02 mm/min (or 3.33 x 10^{-7} m/s) and the pile width (D) of 0.63 m, the Pelect number (Finnie & Randolph 1994) can be computed by:

$$Pelect = \frac{vD}{c_v} \quad (1)$$

The Pelect number is found to be 3.4 x 10^{-6}, which is six orders of magnitude smaller than the threshold value of 1.0, below which shearing may be considered as drained. The lateral pushover was stopped when the pile head displacement reached $0.4D$.

Numerical modelling

140 The soil-pile interaction problem was subsequently analyzed using 3D FE modelling (Fig. 3),
141 employing the numerical analysis code ABAQUS (2017). Owing to the symmetry of the
142 problem, only half of the problem was modelled using prototype dimensions. Initial sensitivity
143 analysis revealed that boundary effects were negligible when the pile was placed at least $8D$
144 away from the sidewall of the container. Accordingly, the modelling domain was reduced
145 compared to the dimensions of the physical model (Fig. 2) to reduce the computational cost.
146 Following the hybrid approach outlined in Anastasopoulos et al. (2013), the pile was
147 modelled with linear beam elements, circumscribed by "dummy" hexahedral brick elements.
148 The nodes of the beam elements representing the pile were rigidly connected with the
149 circumferential brick element nodes at the same height. At each elevation, each beam
150 element had the mechanical properties (E_pI_p and M_{ult}) of the prototype RC pile, while the
151 "dummy" brick elements had negligibly small stiffness and were present to model the correct
152 shape and size of the soil-pile contact surface. Hexahedral brick elements were also used to
153 model the surrounding sand.
154 The soil-pile interface was modelled using the contact elements proposed by
155 Anastasopoulos et al. (2011). These elements connect the nodes of the soil with the
156 corresponding nodes of the pile, which are initially in contact but are allowed to slide on or
157 detach depending on the loading condition. The contact elements are "infinitely" stiff in
158 compression, but they are tensionless, thereby allowing detachment. Following Coulomb's
159 frictional law, the elements are allowed to slide when the frictional capacity is exceeded. A
160 range of friction coefficients ($\tan\delta$) were considered to study the effect of the interface on
161 soil-pile interaction: 10^{-3} (a minimum value to represent "smooth" conditions), 0.6 and 0.87
162 (which was an upper bound for sand-concrete interfaces according to Uesugi et al. 1990). The
163 value of 0.6 was obtained by normalizing the model pile surface roughness by d_{50}, and

matching this ratio to an empirical curve of soil-pile interface friction, after Knappett & Craig (2019).

The bottom boundary of the FE model was constrained in the vertical direction, while only vertical displacement was permitted along the side boundaries. The initial stresses of the pile and the soil were established by "gravity switch-on", meaning that both the pile and the soil establish their initial stress by their self-weight. Hence, the initial effective stress distribution in the simulations of both Test D and S was identical. Since the unit weight between the model pile and the soil was different at prototype scale, relative soil-pile movement was expected in the centrifuges tests. This effect was captured in the FE model. The simulations showed that the relative movement was less than 2.1 mm, which was deemed to be negligible compared to the pile horizontal displacement considered in this study. When simulating Test S, all model boundaries were assumed to be impermeable. The water table was set at the ground surface, generating a hydrostatic distribution of pore water pressure with depth.

Constitutive modelling of the RC pile

Two constitutive approaches were considered, a linear elastic and an elasto-plastic one. The linear elastic model was characterized by the E_pI_p and the Poisson's ratio (v). E_pI_p was set as the upper bound of the measured values (143 MNm^2) from the FPB tests. A typical value of v = 0.2 was assumed, which was reasonable for the used mortar after 28-days of curing (Corinaldesi 2009). In the elasto-plastic model, the elastic component was identical to the elastic model, while the plastic component was defined by a relationship of plastic flexural stress and strain, following the procedures outlined in ASTM C 78: 2002 after the FPB tests. Figure 4 compared the measured (by FPB tests) and predicted bending moment-curvature responses using the two constitutive modelling approaches. The elasto-plastic model

matched reasonably well with the measured nonlinear response. The ultimate (plastic) bending moment of the pile was also captured by this approach. Therefore, the elasto-plastic model was chosen to simulate the pile behavior in sand.

Constitutive models for sand

Three constitutive models of varying degree of sophistication were used to model the sand. The first one was a simple linear-elastic-perfectly-plastic Mohr Coulomb (MC) model with due consideration taken of small-strain stiffness behavior when linearizing the soil stiffness (denoted as LEMC small). In this model, the elastic soil behavior was based on Hooke's law of isotropic elasticity, characterized by v and E $(= G/2\,(1+v))$, where G is the shear modulus), while the plastic response was based on the Mohr-Coulomb failure criterion following a non-associated plasticity framework and was controlled by the three strength parameters, cohesion, friction angle and dilation angle. In this study, a modification was made to consider stress- and strain-dependency of G and linearize the stiffness to capture the small-strain nonlinearity (described below). The second model was an LEMC model that additionally captured post-yield strain-softening (denoted as MC softening). While the elastic part of the model was identical to that of LEMC small, the plastic behavior was characterized by a friction angle and a strain-dependent apparent cohesion. The latter is a cohesion stress-plastic deviatoric strain ($c' - \varepsilon$) curve, where c' was defined by a hyperbolic function (Menétrey 2006 & Willam 1995) of mean effective stress (p') and von Mises deviator stress (q), aiming to capture the post-peak softening behavior observed in triaxial compression tests. The last model was the kinematic hardening model developed by Anastasopoulos et al. (2011).

In both the LEMC small and MC softening models, the elastic sand behavior was characterized by υ and E. To capture the stress-dependency of G in these models, the FE mesh was split into nine sublayers of equal soil thickness. In each sublayer, the initial small-

strain shear modulus of the sand (G_0) was determined as a function of mean effective confining stress (p'):

$$\frac{G_0}{p_{ref}} = A\left(\frac{p\prime}{p_{ref}}\right)^n (\frac{\sigma_e}{p\prime})^m \quad (2)$$

where the state parameter (σ_e) was related to the specific volume (Jovicic & Coop 1997); the parameters A = 38.99, n = 0.593 and m = 0.11 were selected based on fitting shear modulus – shear strain ($G - \gamma$) curves reported by Ishibashi & Zhang (1993) to data from consolidated-drained (CD) triaxial tests for the sand used in the centrifuge tests (D_r = 70%, p'_0 = 20, 40 and 60 kPa); p_{ref} was taken as 60 kPa (i.e., the highest p'_0 for triaxial tests) to make the three parameters dimensionless.

The vertical profile of the effective stress–dependent G_0 was shown in Fig. 5. To approximately capture strain dependency within the framework of linearized elasticity, iterations were carried out to determine the mobilized engineering shear strain (γ) and the corresponding G in each sublayer by applying a lateral load to the pile head. In the first iteration, the profile of G_0 was input and after applying the lateral load, a mobilized γ profile of the soil element immediately in front of the pile at a range of depths (i.e. in the passive zone) was computed. The γ profile was then mapped onto the normalized $G - \gamma$ curve reported by Ishibashi & Zhang (1993) at each depth. A new (mobilized) G was thus obtained (Fig. 6). This mobilized G profile was used in the next iteration and the procedure was repeated until the profiles of input G and resulting strains were consistent with each other. These final mobilized stiffness profiles were then used to extract load-displacement curves for the pile.

For the LEMC small model, stress effects on friction and dilation angles were considered. In each sublayer, the friction and dilation angles were estimated by the empirical relationship

proposed by Bolton (1986). The initial vertical profiles of the friction and dilation angles were identical for both Tests D and S, and they are shown in Figs. 5(c) and 5(d). After applying a lateral load in each iteration (see above), the effective confining pressure in each sublayer changed, hence modifying the friction and dilation angles, though this effect was small.

The MC softening model used the critical-state friction angle and a strain-dependent apparent cohesion. The post-peak softening behavior was captured by inputting a cohesion stress-plastic strain ($c' - \varepsilon$) curve, where c' was defined by a hyperbolic function (Menétrey & Willam 1995) of mean effective stress (p'), von Mises deviator stress (q) and ε is plastic deviatoric strain. This curve was calibrated against the CD triaxial data, and these were input for the different effective confining stresses into sublayers 1-2, 3 and 4-9, respectively.

For the kinematic hardening model, stress-dependency of G_0 was also modelled by Eq. 2, while the strain dependency on stiffness was considered by using an empirical parameter that controlled the sand nonlinearity (λ), which ranges from 0.1 to 0.3 for sand (Anastasopoulos et al. 2011). In this study, λ was set 0.3 after calibration against the $G/G_0 - \gamma$ curve of Fig. 6. This model used an extended von Mises failure criterion by introducing a kinematic term on stress controlled by its hardening rate. The yield stress was related to the effective confining stress (p') and friction angle (ϕ) as $\sqrt{3}p' \sin\phi$.

Figure 7 compares the deviator stress-axial strain relationships of the three models with measurements from the CD triaxial compression tests conducted at p'_0 = 40 kPa (Robinson 2016), as a typical example. Comparisons with the triaxial test data at p'_0 = 20, 40 and 60 kPa were conducted. In the triaxial tests, the deviatoric stress mobilized nonlinearly before reaching peak stress, followed by strain-softening towards a critical-state value of the deviator stress. The LEMC small model captured well both the initial stiffness and the peak stress, but it was unable to model the non-linear response at higher strains or the post-peak

softening behavior. The kinematic hardening model improved on this, capturing well the nonlinear response at relatively small-strains (before the peak), but also could not simulate the strain-softening behavior at large strains. The MC softening model reproduced the triaxial response well, at all three levels of p'_0 considered.

Results and discussion

Figure 8(a) compared the measured and predicted lateral load-displacement curves of the RC model pile in dry (Test D) and saturated (Test S) sand, using the MC softening model. The analysis exhibited typical hardening behavior in all cases. The model pile displayed a nonlinear increase in lateral load with lateral displacement, and yielded for $y > 0.08D$. The FE simulation shows that the pile has reached the maximum bending moment and developed a plastic hinge at $y = 0.02D$. The simulation also realistically mimicked the effects of the quasi-brittle behavior that would be expected for the prototype RC pile subjected to lateral loading. The initial stiffness and the ultimate load for dry and saturated sand were similar (Fig. 8(a)). This was not a surprise, as the two tests were intentionally performed at different g-levels in order to create identical effective stress regimes. The discrepancies of load for $0.06D < y < 0.36D$ were likely associated with material variabilities of the model RC between the two piles (Knappett et al. 2018; Zhao et al. 2020).

Figure 8(a) also compared the computed load-displacement curves for different soil-pile interface friction coefficients, all using the MC softening model. As it would be expected, the increase of the interface friction coefficient led to a stiffer response and a higher ultimate lateral pile capacity. Most importantly, using the value that was consistent with the roughness measurements ($\tan\delta = 0.6$), predicted the measured load-displacement curve well.

Figure 8(b) compared the load-displacement curves predicted by the three different soil constitutive models, all with an interface friction coefficient of 0.6. In terms of initial stiffness,

283 the predictions made by the LEMC small and MC softening model were similar and were close
284 to the measurements. The kinematic model however predicted a higher initial stiffness. The
285 curves predicted by both the LEMC small and MC softening started to deviate from the
286 measurement at a displacement of approximately y = 0.08D (i.e., at yield), with the latter
287 model achieving a better prediction of the measured response, though the difference was
288 small. This suggested that for the laterally-loaded pile problem, the load-displacement
289 response could be well approximated by models which did not incorporate strain softening,
290 even though soil behavior did exhibit a strong softening response (Figure 7). Indeed, stress
291 paths of soil elements extracted from the passive zone (i.e. ahead of the displacing pile) in the
292 FE calculation showed monotonic increased throughout the loading.

293 Figure 9 showed post-test observations of the cracked pile and the FE-computed pile
294 deflection, bending moment, shear force and limiting lateral pressure for Test D, predicted by
295 the MC softening model. The model RC pile displayed prominent flexural cracks at 1.05 m
296 depth (prototype) below the ground surface, where a plastic hinge was formed (Fig. 9(a)). This
297 was fairly close to the FE-computed depth of 1.19 m, where maximum bending moment (Fig.
298 9(c)) and zero shear force (Fig. 9(d)) was observed. Figure 9(b) shows the computed elastic
299 critical length (L_c), at which the pile deflection become zero which was 3.6 m below the soil
300 surface. This compared well with the theoretical value of 3.9 m, estimated according to
301 Randolph (1981), in which an approximate linear G-depth relationship was assumed.

302 Figure 10 showed the distributions of pile deflection, bending moment, shear force and
303 limiting lateral pressure with depth for the Test S, predicted by the MC softening model. The
304 measured plastic hinge position was 1.12 m and consistent with where the FE-computed
305 maximum bending moment and zero shear force occurred. The difference of this value
306 between that in dry test was due to material variability of two piles, although it was negligible.

The ultimate lateral pile capacity (P_{ult}) obtained from the centrifuge tests (i.e., 120 kN) was compared to existing analytical methods and the FE simulations. The pile was long and flexible since the relative pile-soil stiffness, expressed as E_pI_p/E_sL^4 (where E_s is the Young's modulus of soil, and L is the pile length; Meyerhof & Yalcin 1984), was less than 0.01. The first semi-empirical method was proposed by Broms (1964), who assumed (1) the limiting lateral soil pressure (p_u) to be linearly proportional to soil depth, and proportional also to $3K_p$ (where K_p is the passive earth pressure coefficient); (2) soil below the plastic hinge (at a depth of f) did not contribute; and (3) the interface was frictionless. Based on these assumptions, P_{ult} could be assessed from the moment capacity of the pile ($M_{max} = 225\ kNm$), the pile upstand above the ground (e; i.e., 1.75 m), the effective unit weight of the dry sand (γ'; i.e., 16.5 kN/m^3) and $K_p = 3.3$ using Rankine's theory with $\phi' = \phi_{crit} = 32°$:

$$K_p = \frac{1+sin\phi'}{1-sin\phi'} \quad (3)$$

while the relationship between P_{ult} and f is:

$$f = 0.82\sqrt{\frac{P_{ult}}{\gamma' D K_p}} \quad (4)$$

Hence, P_{ult} predicted using the Broms' method was 80 kN, with a plastic hinge depth of $f = 1.6\ m$. Using instead the average peak friction angle of $\phi' = 41°$ (Figure 5(b)) resulted in $K_p = 4.8$, and $P_{ult} = 84\ kN$ for $f = 1.35\ m$. This method underestimated the measured P_{ult} in the centrifuge by approximately 37% and 34%, respectively, and predicted a deeper plastic hinge depth than was observed.

A second existing approach that could be used to estimate P_{ult} was the that presented in the form of design charts in Fleming et al. (2009), which assumed p_u to be proportional to K_p^2. Using $K_p = 3.3\ or\ 4.8$, P_{ult} was determined as 86 or 100 kN, respectively.

In the FE simulations the limiting lateral pressure distribution increased initially much more rapidly with depth compared to Broms' prediction (Figs 9(e) and 10(e)). The computed pressures increased up to a maximum value of 34 – 44 $\gamma' D$ (saturated and dry cases, respectively) at a depth of $0.25 - 0.5f$, then decreased to 13 – 15 $\gamma' D$ at f (the plastic hinge; Figs 9(e) and 10(e)). The initial steeper increase in lateral pressure was thought to be due to a higher value of K_p due to the rough interface (the previous methods used K_p from Equation (1) which is consistent with smooth interface conditions). Based on lower-bound plasticity analysis, the value of K_p against a vertical interface with interface friction angle of δ can be determined using:

$$K_p = \frac{1+sin\phi' cos(\Delta+\delta)}{1-sin\phi'} e^{(\Delta+\delta)tan\phi'} \quad (5)$$

(e.g. Knappett and Craig 2019), where:

$$sin\Delta = \frac{sin\delta}{sin\phi'} \quad (6)$$

For $tan\,\delta$ = 0.6, $K_p = 5.8$ for $\phi' = 32°$ and $K_p = 11.0$ for $\phi' = 41°$.

For analytical (design) calculations, an alternative simplified bi-linear lateral pressure distribution was proposed as an alternative to that of Broms (1964), where $p_u/(\gamma' zD) = K_p^2$ from the surface to a depth of $z = \eta f$ and then reduces linearly from this peak value back to $p_u = 0$ at $z = f$. The unknown value of f was determined assuming $\eta = 0.25$ by trial and error (or using an optimization routine) to ensure that the resultant moment generated about the plastic hinge position by this pressure distribution (i.e. $\Sigma p_u(f - z)$, computed numerically within a spreadsheet) was equal to the plastic hinge capacity to satisfy moment equilibrium. Using $K_p = 11.0$ for $\phi' = 41°$ gave $f = 1.05\,m$ and $\eta = 0.24$. Then, from horizontal equilibrium $P_{ult} = 103\ kN$, an underprediction by 19%. The resulting pressure distribution is

shown on Figs 9(e) and 10(e) and demonstrates the importance of incorporating the roughness effect on K_p in obtaining a representative lateral earth pressure distribution.

The new bi-linear method proposed above, while still underpredicting the measured and numerically simulated capacities (conservative in ultimate limit state design), has reduced the error in P_{ult} by approximately half compared to the Broms' method and also better predicts the location of the plastic hinge and the lateral pressure distribution (which may be useful in the structural detailing of the pile). It achieves this while being little more computationally difficult than the original Broms' method (the procedure presented here being a numerical implementation of the Broms' solution method for unknown f and P_{ult}).

Summary and conclusions

This study has demonstrated the effectiveness of using small-scale model reinforced concrete (RC) to realistically reproduce the flexural behavior of a laterally-loaded RC pile in sand within a geotechnical centrifuge. A 10.5 m-long pile in uniform sand of D_r = 67% was laterally loaded up to a displacement of 0.4D. The model pile initially exhibited linear elastic response and as tension cracks developed, a plastic hinge was formed. Based on the observed post-test deformation shape and crack pattern of the model RC pile, the nonlinear quasi-brittle characteristics of a prototype RC pile were closely resembled, which would not have been possible using an elastic model pile.

Three-dimensional FE simulation was conducted to investigate the nonlinear response of the laterally loaded pile (after initially being validated against the centrifuge tests in terms of the global pile lateral response). Three different soil constitutive models were considered, from simple elastic-perfectly plastic, to kinematic strain hardening, and a strain softening model. It was demonstrated that, at least for the problem studied herein, the strain-softening response observed in triaxial soil element tests was not crucial in simulating the pushover

response of the pile. An iterative approach was developed to incorporate the effects of soil stiffness non-linearity in simpler linear elastic-perfectly plastic models in terms of an equivalent mobilized shear modulus and a sublayer approach. This was shown to be of importance in order to capture the pre-peak load-deformation response of the pile correctly, and when implemented allowed the simplest of the constitutive models (available in all commercial FE software) to replicate the observed pile behavior well, requiring only routine strength and unit weight parameters, G_0 values and an appropriate $G - \gamma$ curve as input.

Broms' popular method underestimated the ultimate lateral capacity by approximately 35% compared to measurements and simulations, and overpredicted the depth of the plastic hinge. An improved method was proposed, based on the Broms' approach but using a simple bi-linear soil lateral pressure distribution. This gave a better (though still conservative) prediction of capacity while also more accurately predicting the plastic hinge depth and the shape/magnitude of the lateral pressure distribution at failure. This proposed approach should allow for improved (more optimal) design and detailing at the ultimate limit state.

Data availability statement

Some or all data, models, or code that support the findings of this study are available from the corresponding author upon reasonable request.

Acknowledgments

The corresponding (second) author would like to acknowledge the funding provided by the National Natural Science Foundation of China (NSFC) under the Excellent Youth Scientist Scheme (H. K. & Macau) (project no. 51922112). The first author would also like to acknowledge Basic Science Center Program for Multiphase Media Evolution in Hypergravity of the NSFC (no. 51988101) and the grants (no. 51922112 and no. 51625805), the studentship provided by the Chinese Scholarship Council as well as the support from the Department of

399 Civil, Environmental and Geomatic Engineering, ETH Zürich during a 3-month research visit.
400 The authors sincerely thank Prof. Ioannis Anastasopoulos and Dr Alexandru Marin from ETH
401 Zürich for his contribution to the setup of the numerical models and parameter calibration.

402 **References**

403 Al-Baghdadi, T., Brown, M. J., and Knappett, J. A. (2017). “Effects of vertical loading on lateral
404 screw pile performance.” *Proc. Inst. Civ. Eng. Geotech. Eng.,* 170(3), 259-272.
405 Al-Defae, A. H., Caucis, K. and Knappett, J. A. (2013). “Aftershocks and the whole-life seismic
406 performance of granular slopes”. *Géotechnique,* 63(14), 1230-1244.
407 Al-Defae, A. H., and Knappett, J. A. (2014). “Centrifuge modeling of the seismic performance
408 of pile-reinforced slopes.” *J. Geotech. Geoenviron. Eng., ASCE*, 140(6), p.04014014.
409 Anastasopoulos, I., Gelagoti, F., Kourkoulis, R. and Gazetas, G. (2011). “Simplified constitutive
410 model for simulation of cyclic response of shallow foundations: validation against
411 laboratory tests”. *J. Geotech. Geoenviron. Eng.*, 137(12), 1154-1168.
412 Anastasopoulos, I., Kourkoulis, R., Gazetas, G. and Tsatsis, A. (2013). “Interaction of piled
413 foundation with a rupturing normal fault”. *Géotechnique,* 63(12), 1042-1059.
414 ASTM, C., 2002. 78-02. Standard Test Method for Flexural Strength of Concrete (Using Simple
415 Beam with Third-Point Loading).
416 Bhattacharya, S., Lombardi, D. and Wood, D. M. (2011). “Similitude relationships for physical
417 modelling of monopile-supported offshore wind turbines.” *Int. J. of Phys. Modell. in*
418 *Geotech.*, 11, 58-68.
419 Bolton, M. D. (1986). “Strength and dilatancy of sands”. *Géotechnique,* 36(1), 65-78.
420 Bolton, M. D. (1991). *A Guide to Soil Mechanics,* Macmillan Press, London.
421 Bolton, M. D., Gui, M. W., Garnier, J., Corte, J. F., Bagge, G., Laue, J. and Renzi, R. (1999).
422 Centrifuge cone penetration tests in sand. *Géotechnique*, 49(4), 543-552.

Brennan, A. J., Knappett, J. A., Bertalot, D., Loli, M., Anastasopoulos, I. and Brown, M. J. (2014). "Dynamic centrifuge modelling facilities at the University of Dundee and their application to studying seismic case histories". *Proc. Int. Conf. on Phys. Modell. in Geotech.*, U. K., 227-233.

Broms, B. B. (1964). "Lateral resistance of piles of cohesionless of soils". *J. Soil Mech. Found. Div.*, 90(3), 123-158.

Corinaldesi, V. (2009). "Mechanical behavior of masonry assemblages manufactured with recycled-aggregate mortars". *Cem. Concr. Compos.* 31(7), 505-510.

Fleming, K., Weltman, A., Randolph, M. and Elson, K. (2009). *Piling engineering, 3rd Edition.* CRC press.

Finnie, I. M. S., and Randolph, M. F. (1994). Punch-through and liquefaction induced failure of shallow foundations on calcareous sediments. *In Seventh International Conference on the Behaviour of Offshore Structures*, 1: 217-230.

Goode, J., III., and McCartney, J. S. (2015). "Centrifuge modeling of boundary restraint effects in energy foundations." *J. Geotech. Geoenviron. Eng., ASCE*, 141(8), p.04015034.

Iai, S., Tobita, T. and Nakahara, T., (2005). "Generalised scaling relations for dynamic centrifuge tests". *Géotechnique,* 55(5), 355-362.

Ishibashi, I. and Zhang, X. (1993). "Unified dynamic shear moduli and damping ratios of sand and clay." *Soils Found.,* 33(1), 182-191.

Ito, K., Ohno, S., and Matsuda, T. (2006). "Seismic response of underground reinforced concrete structure—Centrifuge model test and its analysis." *J. Earthquake Eng.,* 23(1), 117–124.

Jovicic, V. and Coop, M. R. (1997). "Stiffness of coarse-grained soils at small strains". *Géotechnique,* 47(3), 545-561.

447 Knappett, J. A., Brown, M. J., Shields, L., Al-Defae, A. H. and Loli, M. (2018). “Variability of
448 small scale model reinforced concrete and implications for geotechnical centrifuge
449 testing”. *Proc. Int. Conf. on Phys. Modell. in Geotech.*, U. K.*,* 1, 241-246.
450 Knappett, J. A. and Craig, R. F. (2019). *Craig's soil mechanics, 9th Edition.* CRC press.
451 Knappett, J. A., Reid, C., Kinmond, S., and O’Reilly, K. (2011). “Small-Scale Modeling of
452 Reinforced Concrete Structural Elements for Use in a Geotechnical Centrifuge.” *J. Struct.*
453 *Eng. ASCE,* 137(11), 1263-1271.
454 Li, Z., Haigh, S. K. and Bolton, M. D. (2010). “Centrifuge modelling of mono-pile under cyclic
455 lateral loads.” *Proc. Int. Conf. on Physical Modelling in Geotechnics*, Zurich*,* 2, 965-970.
456 Menétrey, P. and Willam, K. J. (1995). “Triaxial Failure Criterion for Concrete and its
457 Generalization”. *Struct. J.,* 92, 311–318.
458 Meyerhof, G. G., and Yalcin, A. S. (1984). “Pile capacity for eccentric inclined load in clay.”
459 *Can. Geotech. J.,* 21, 389-396.
460 Randolph, M. F. (1981). “The response of flexible piles to lateral loading”. *Géotechnique,*
461 31(2), 247–259.
462 Robinson, S. (2016). “NorSand Parameter Characterisation for CN HST95 Sand – Seabed
463 Ploughing: Modelling for Infrastructure Installation.” *Internal Report,* University of
464 Dundee, UK.
465 Taylor, R. N. (1995). *Geotechnical centrifuge technology*. Taylor and Francis.
466 Uesugi, M., Kishida, H. and Uchikawa, Y. (1990). “Friction between dry sand and concrete
467 under monotonic and repeated loading”. *Soils Found.,* 30(1), 115-128.
468 Vitali, D., Leung, A. K., Minto, A. and Knappett, J. A. (2016). “A New Model Concrete for
469 Reduced-Scale Model Tests of Energy Geo-Structures”. In *Geo-Chicago,* 185-194.
470 Zhang, L., McVay, M. C. and Lai, P. W. (1999). “Centrifuge modelling of laterally loaded single

471 battered piles in sands.” *Can. Geotech. J.,* 36(6), 1074-1084.

472 Zhao, R., Leung, A. K., Vitali, D., Knappett, J. A. and Zhou, Z. (2020). “Small-Scale Modelling of

473 Thermomechanical Behavior of Reinforced Concrete Energy Piles in Soil.” *J. Geotech.*

474 *Geoenviron. Eng.*, *.ASCE*, 146(4): 04020011

Table 1. Summary of relevant scale factors (i.e., *N* = prototype/model, equal to 35 for both Tests D and S) for flexural soil-structure interaction problems in high-g (after Iai et al. 2005)

Quantity	Scale factor
Length	N
Density	1
Stress	1
Strain	1
Stiffness (of soil)	1
Bending stiffness (E_pI_p)	N^4
Bending moment (M_{ult})	N^3
Force	N^2
Displacement	N

Table 2. Index and mechanical properties of the HST95 silica sand used in the centrifuge tests

Parameter	Value
Specific gravity, G_s	2.63
Maximum void ratio, e_{max}	0.769
Minimum void ratio, e_{min}	0.467
Mean grain diameter, d_{50} (mm)	0.13
Coefficient of uniformity, C_u	1.9
Coefficient of curvature, C_z	1.06
Critical friction angle, ϕ_{crit} (°)	32
Peak friction angle[a], ϕ_{peak} (°)	42
Dilation angle[a], ψ (°)	12
Effective unit weight, γ' (kN/m^3)	10.15
Poisson's ratio	0.32

Note: [a]Measured for dense sand over p_0' = 20 to 60 kPa (Robinson, 2016).

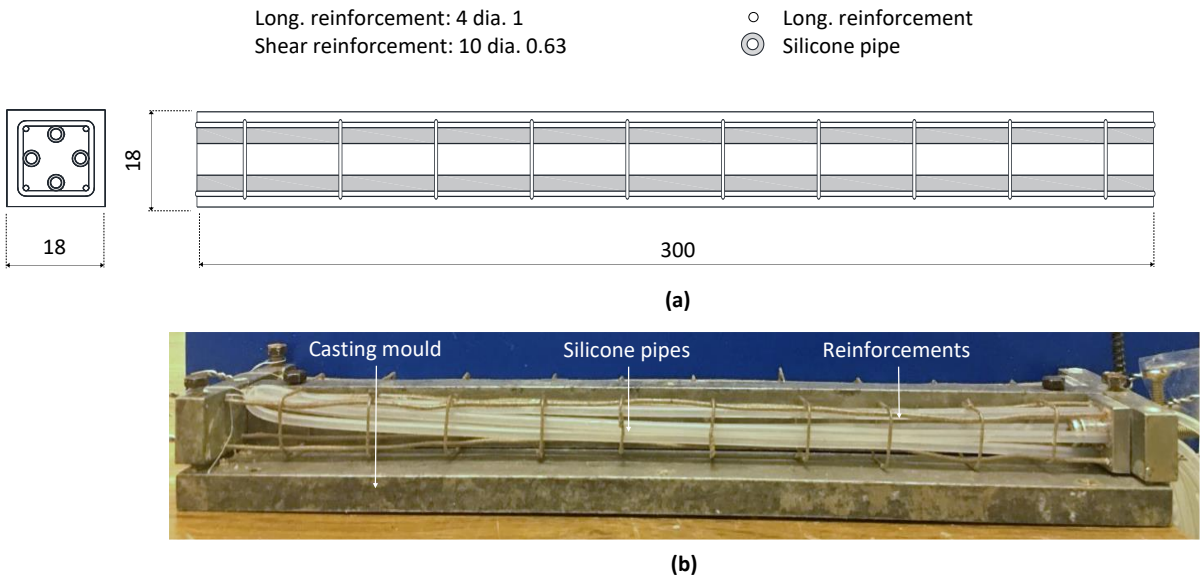

Figure 1. Model RC pile: (a) geometry and reinforcement details; and (b) picture showing the arrangement of circulation pipes and steel reinforcement. All dimensions in mm (model scale).

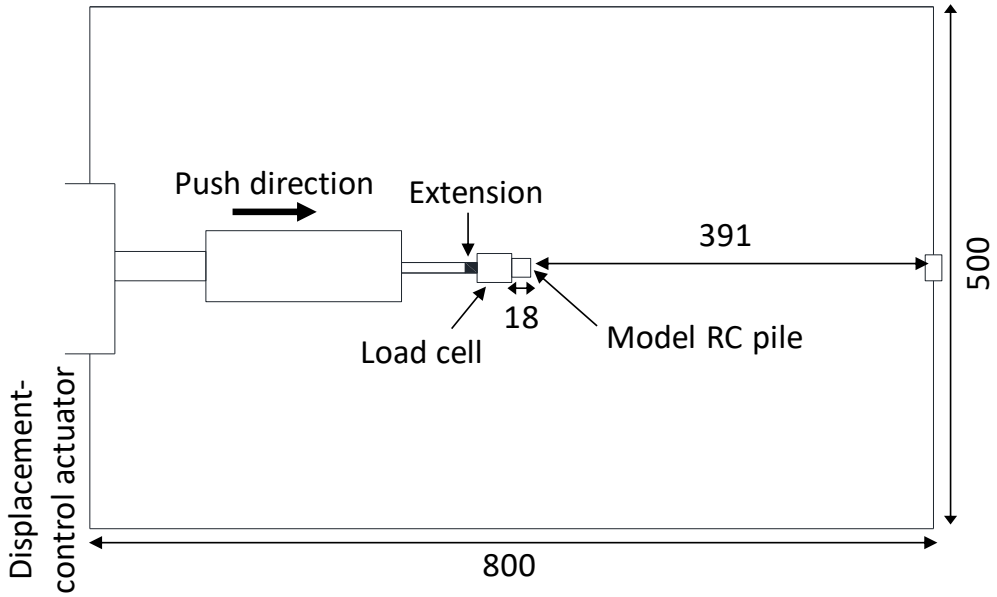

(a)

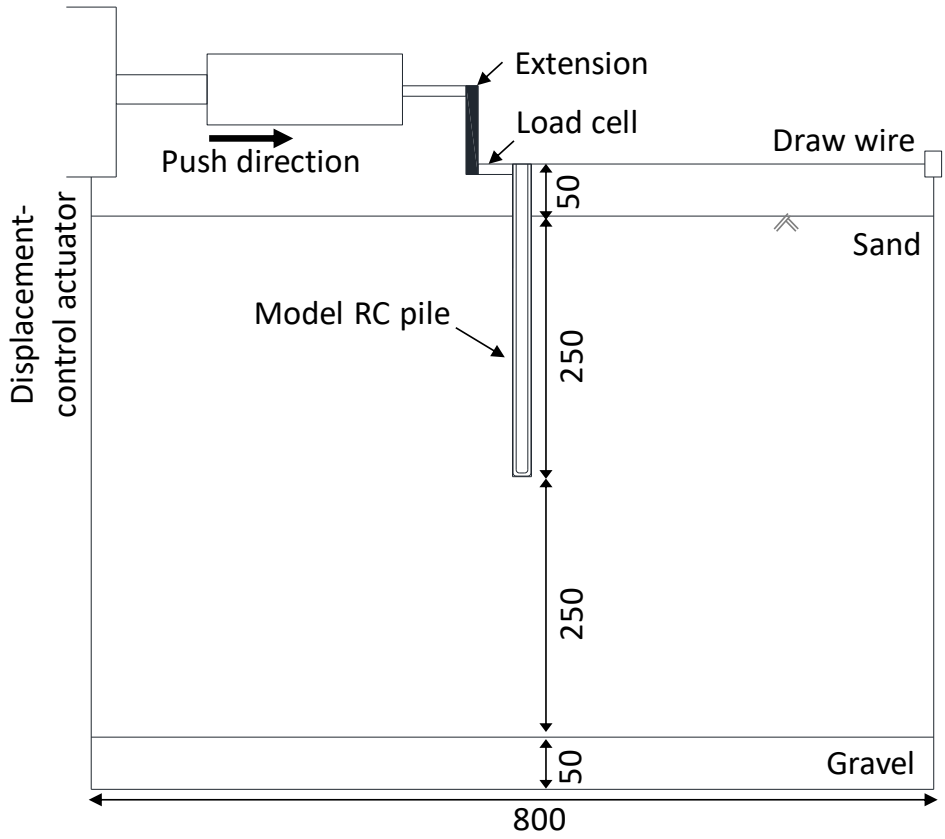

(b)

Figure 2. Centrifuge model setup: (a) plan; and (b) elevation view. All dimensions in mm (model scale).

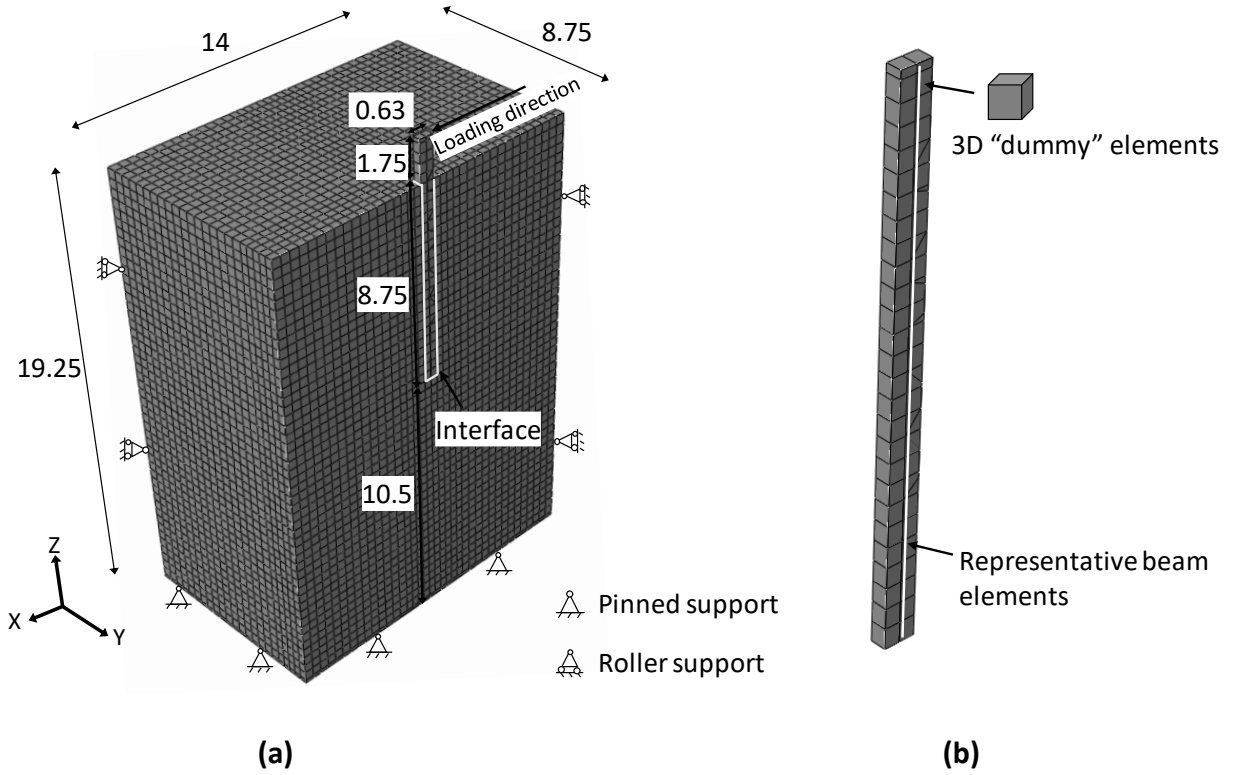

Figure 3. 3D finite element model: (a) mesh and boundary conditions; and (b) "hybrid" pile modelling (Anastasopoulos et al. 2013). All dimensions in m (prototype scale)

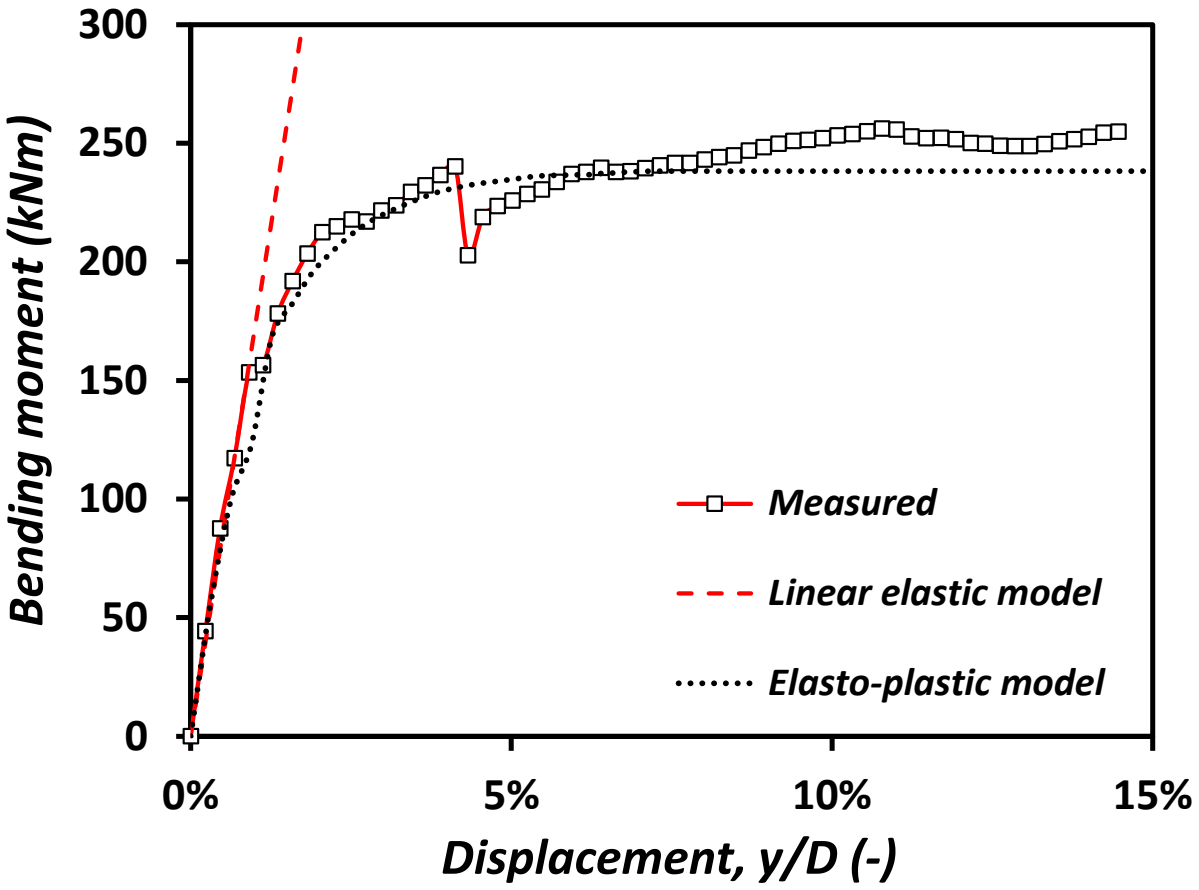

Figure 4. Comparison of measured and predicted moment-displacement relationships of the model RC pile (expressed in prototype scale, following the scaling laws of Table 1).

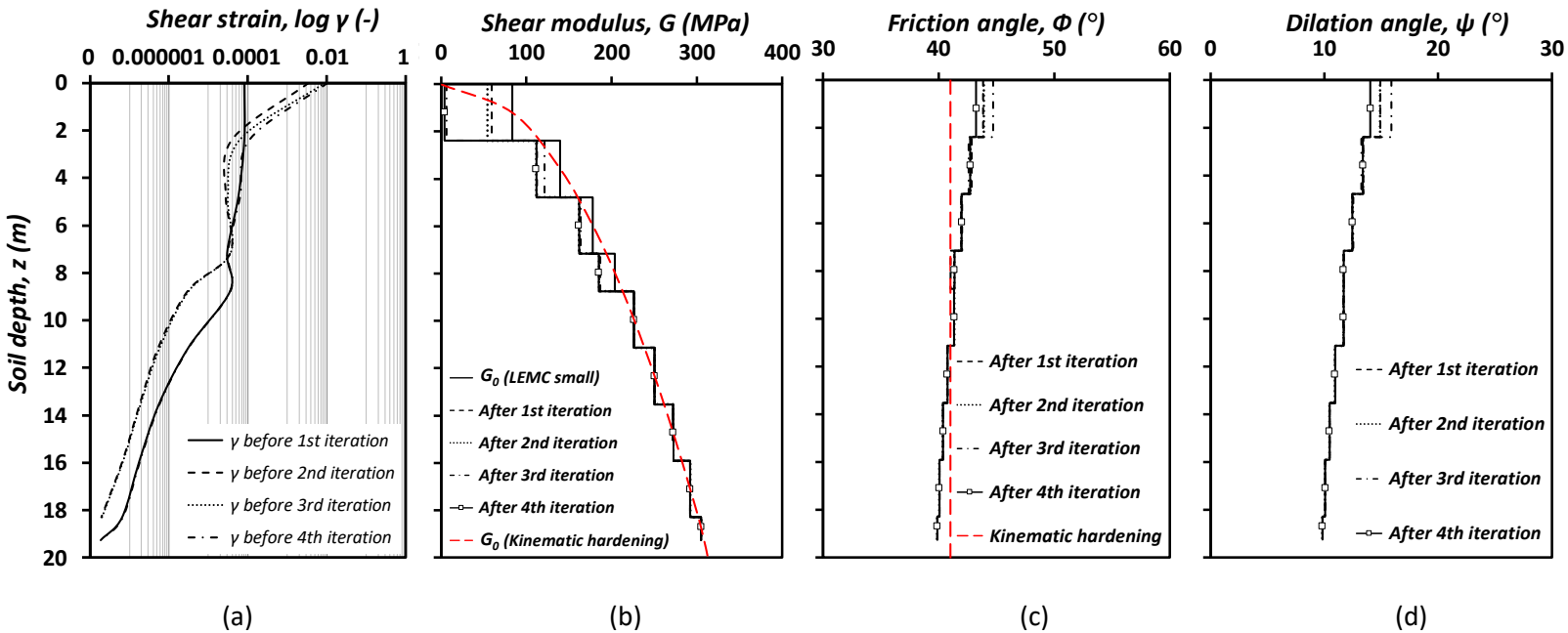

Figure 5. Calibrations: distributions of (a) engineering shear strain (γ); (b) shear modulus; (c) friction angle; and (d) dilation angle with depth for Test D, as an example.

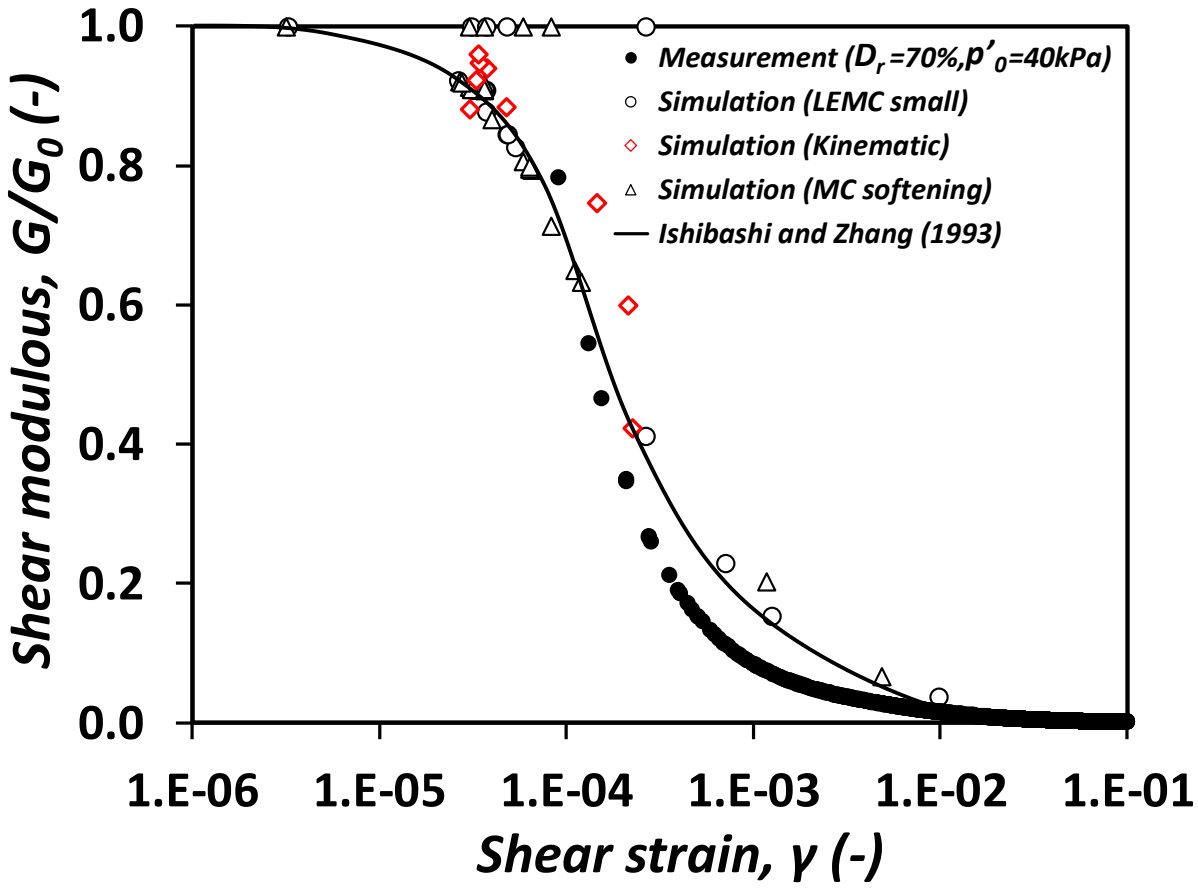

Figure 6. $G-\gamma$ curves after calibration of the small-strain parameters of each constitutive soil model.

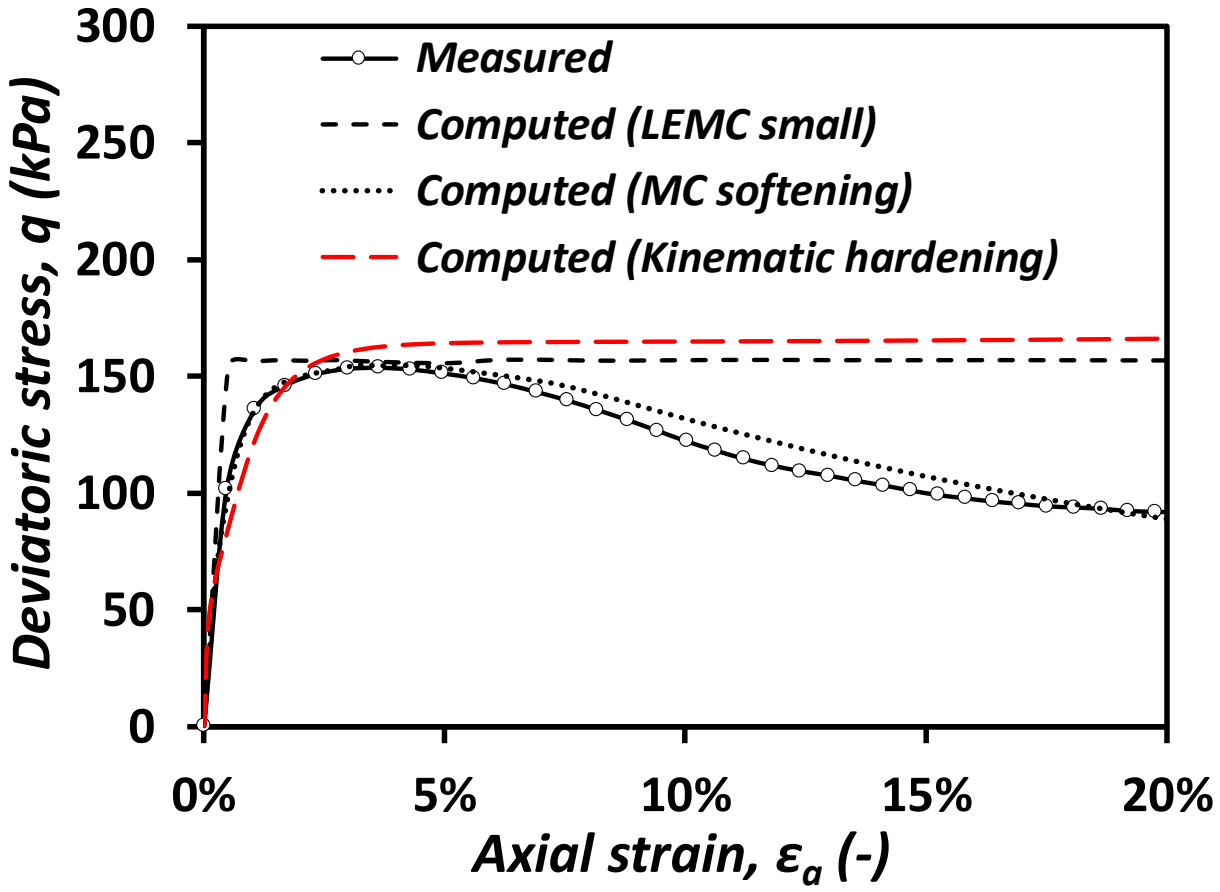

Figure 7. Calibrations of deviatoric stress-axial strain curves against the measured data for dense sand (D_r = 70%) in a consolidated-drained triaxial compression test at p_0' = 40 kPa.

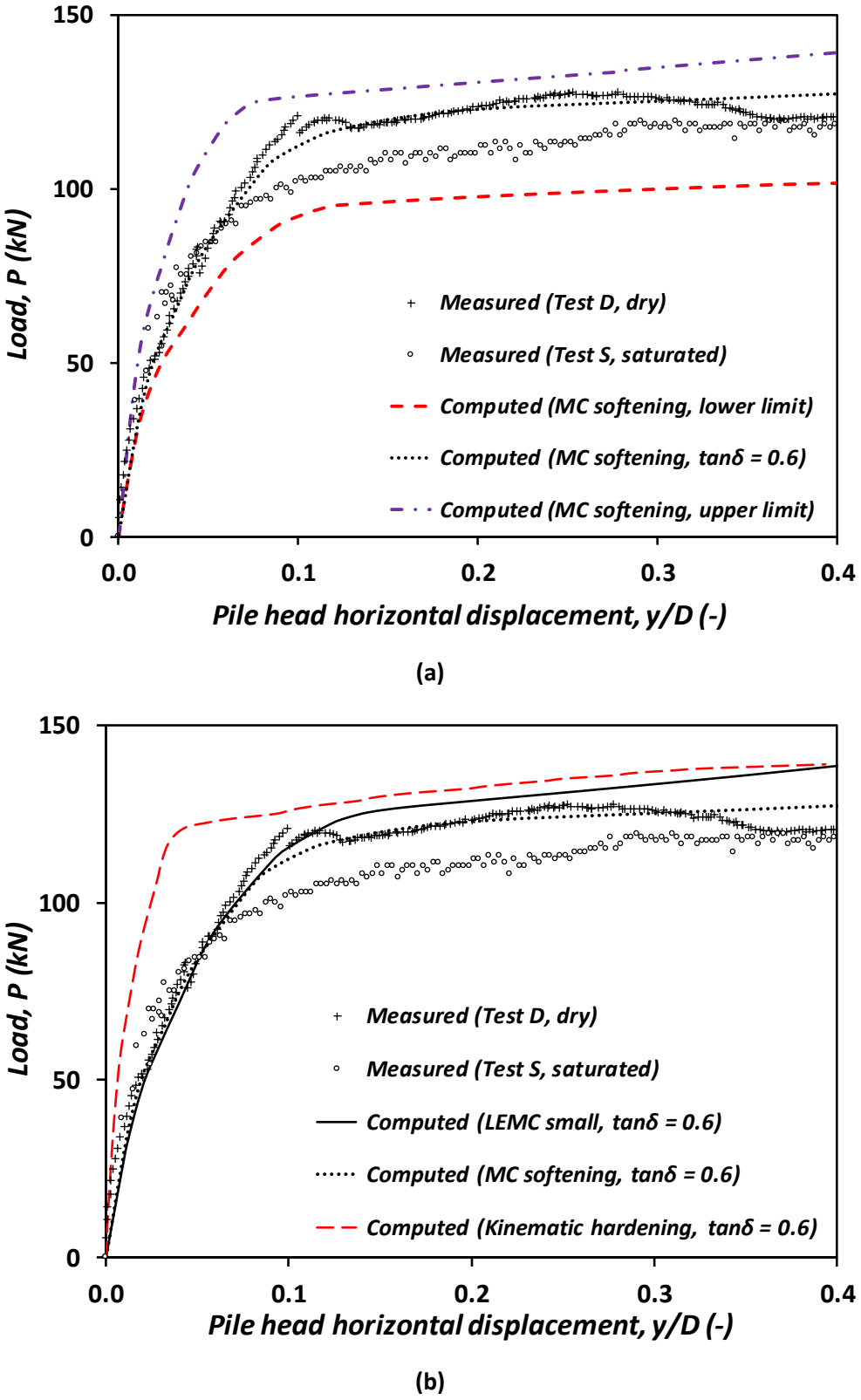

Figure 8. Effects of (a) soil-pile interface friction coefficient; and (b) constitutive soil models on the prediction of the load-displacement curves of a laterally-loaded RC pile, at prototype scale

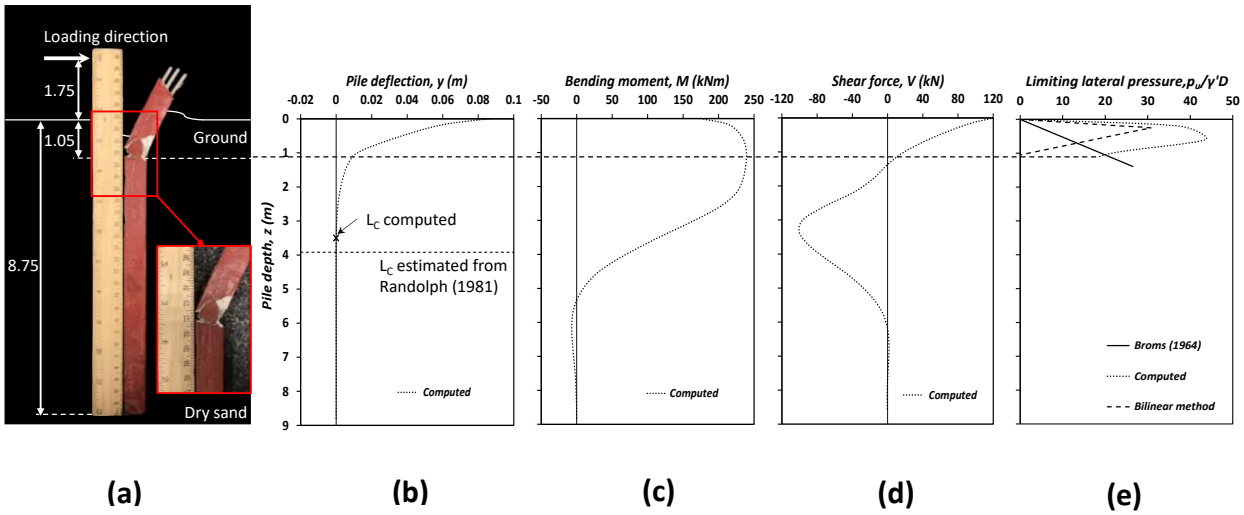

Figure 9. (a) Overview of a cracked laterally-loaded RC model pile after testing (dimensions in m, prototype scale). Distributions of FE-computed (b) pile deflection (c) bending moment (d) shear force and (e) limiting lateral soil pressure above the plastic hinge with depth for Test D, all expressed in prototype scale.

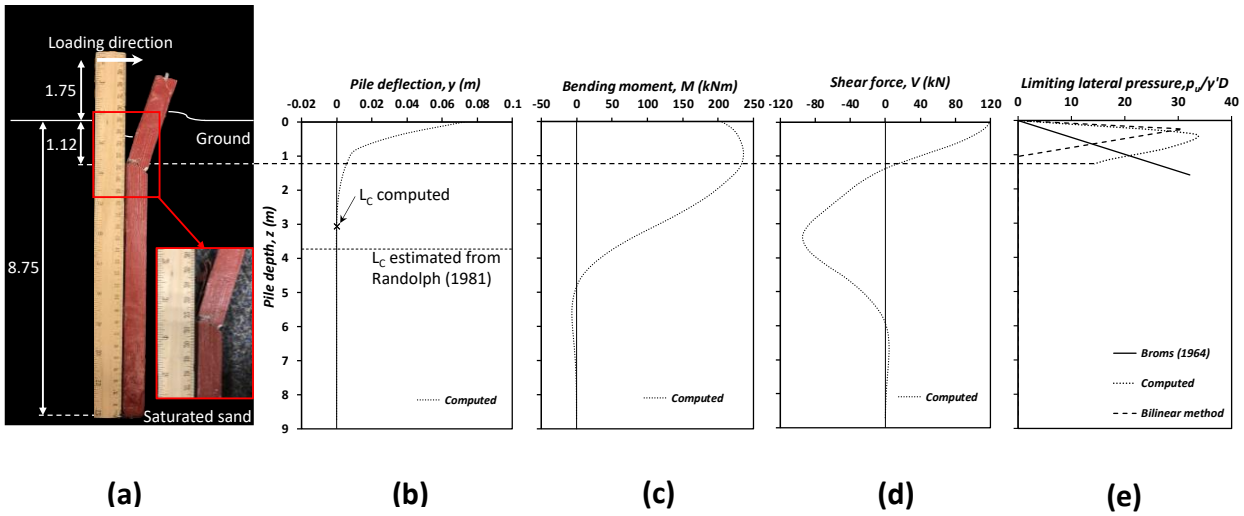

Figure 10. (a) Overview of a cracked laterally-loaded RC model pile after testing (dimensions in m, prototype scale). Distributions of FE-computed (b) pile deflection (c) bending moment (d) shear force and (e) limiting lateral soil pressure above the plastic hinge with depth for Test S, all expressed in prototype scale.

List of table captions

Table 1. Summary of relevant scaling factors (i.e., *N* = prototype/model, equal to 35 for both Tests D and S) for flexural soil-structure interaction problems in high-g (after Iai et al. 2005)

Table 2. Index and mechanical properties of the HST95 silica sand used in the centrifuge tests

List of figure captions

Figure 1. Model RC pile: (a) geometry and reinforcement details; and (b) picture showing the arrangement of circulation pipes and steel reinforcement. All dimensions in mm (model scale)

Figure 2. Centrifuge model setup: (a) plan; and (b) elevation view. All dimensions in mm (model scale).

Figure 3. 3D finite element model: (a) mesh and boundary conditions; and (b) "hybrid" pile modelling (Anastasopoulos et al. 2013). All dimensions in m (prototype scale)

Figure 4. Comparison of measured and predicted moment-displacement relationships of the model RC pile (expressed in prototype scale, following the scaling laws of Table 1)

Figure 5. Calibrations: distributions of (a) engineering shear strain (γ); (b) shear modulus; (c) friction angle; and (d) dilation angle with depth for Test D, as an example

Figure 6. $G-\gamma$ curves after calibration of the small-strain parameters of each constitutive soil model

Figure 7. Calibrations of deviatoric stress-axial strain curves against the measured data for dense sand (D_r = 70%) in a consolidated-drained triaxial compression test at p'_0 = 40 kPa

Figure 8. Effects of (a) soil-pile interface friction coefficient; and (b) constitutive soil models on the prediction of the load-displacement curves of a laterally-loaded RC pile, at prototype scale

Figure 9. (a) Overview of a cracked laterally-loaded RC model pile after testing (dimensions in m, prototype scale). Distributions of FE-computed (b) pile deflection (c) bending moment (d) shear force and (e) limiting lateral soil pressure above the plastic hinge with depth for Test D, all expressed in prototype scale

Figure 10. (a) Overview of a cracked laterally-loaded RC model pile after testing (dimensions in m, prototype scale). Distributions of FE-computed (b) pile deflection (c) bending moment (d) shear force and (e) limiting lateral soil pressure above the plastic hinge with depth for Test S, all expressed in prototype scale